Astron. Astrophys. 351, 1115–1132 (1999)

ASTRONOMY AND ASTROPHYSICS

A study of extreme ultraviolet blinker activity

R.A. Harrison[1], **J. Lang**[1], **D.H. Brooks**[2], **and D.E. Innes**[3]

[1] Space Science Department, Rutherford Appleton Laboratory, Chilton, Didcot, Oxfordshire OX11 0QX, UK
[2] Centro de Astrofisica da Universidade do Porto, Rua das Estrelas s/n, 4150-Porto, Portugal
[3] Max-Planck-Institut fur Aeronomie, 37191 Katlenburg-Lindau, Germany

Received 16 June 1999 / Accepted 15 September 1999

Abstract. In a previous paper (Harrison, 1997a), we reported on the existence of extreme ultraviolet (EUV) flashes, known as blinkers, which were identified in the quiet Sun network using the CDS instrument on board the Solar and Heliospheric Observatory. Since then a number of dedicated observations have been made and we report here on an analysis of 97 blinker events. We identify blinker spectral, temporal and spatial characteristics, their distribution, frequency and general properties, across a broad range of temperatures, from 20,000 K to 1,200,000 K. The most significant brightenings were found in the transition region temperature lines of O III, O IV and O V, with modest or no detectable increases at higher or lower temperatures. A typical blinker event has a duration of order 1000 s, though the detection of short-duration blinkers may well be limited by the observation methods. However, a long tail of longer-duration blinkers puts the average blinker duration at almost 2400 s. Comparisons to plasma cooling times establish firmly that there is a continuous energy input throughout the blinker event. The projected blinker onset rate for the entire solar surface is $1.24\,s^{-1}$ i.e. 3,000 blinker events may be in progress at any point in time. An examination of the line ratios shows a remarkable feature. Ratios of lines from O III, O IV and O V show no significant change throughout the blinker event and this indicates that the blinkers are predominantly caused by inceases in density or filling factor. The intensity signatures of the blinkers are modelled using a basic time dependent code and this confirms that the lack of a change in the oxygen line ratios is consistent with a density or filling factor increase in a plasma cooling from a temperature above 5×10^5 K. We estimate the thermal energy content of an average blinker at 2×10^{25} erg and consider this figure and the total blinker rate in the light of the energy required for coronal heating. The results are used to compare blinker activity to reported micro-flare, network flare and explosive event activity, and to discuss their potential role in coronal heating and solar wind acceleration processes. Finally, a blinker model is presented which consists of the merging of a closed magnetic system with pre-existing open field lines in the network.

Key words: Sun: activity – Sun: atmosphere – Sun: transition region – Sun: UV radiation

Send offprint requests to: R.A. Harrison

1. Introduction

Recently, Harrison (1997a, 1997b) reported the existence of transient extreme ultraviolet (EUV) flashes or brightenings detected primarily at what we think of as transition region temperatures, in the quiet Sun network. These events have become known as blinkers and a rough projection of the initial observations suggested that several thousand blinkers may be occurring at any point in time, distributed throughout the solar surface. It was surmised from the initial results that these may be indicative of sites in the solar atmosphere where magnetic mergence due to convective flow leads to transient events through magnetic reconnection/reformation which in turn generated acceleration and particle heating. The relevance of this to the outstanding problems in our understanding of solar coronal heating and solar wind acceleration were noted.

Here, we present a detailed analysis of a large set of EUV blinker events identified in a set of dedicated observations made in 1997–8. This analysis provides a view of the general properties of these events and thus can be used to determine their role in the solar atmosphere, in particular in relation to coronal heating and solar wind acceleration. We compare these observations to EUV intensity variations observed by Vernazza et al. (1975) using Skylab as well as quiet Sun transient phenomena reported at differing wavelengths, such as explosive events, network flares and microflares, reported by Innes et al. (1997), Porter et al. (1987), Krucker et al. (1997), Benz and Krucker (1998) and Berghmans et al. (1998).

In the next section we outline the observation technique and the observing runs. This is followed by a detailed analysis of one period. We then perform a statistical analysis of the entire 97 event dataset. The blinker properties are then summarised and in the ensuing discussion we make the comparison to other quiet Sun transient phenomena and investigate the impact of the blinker activity on the solar atmosphere. A preliminary model is presented.

2. The observations

We report here on results from 11 sequences observing the quiet Sun using the Coronal Diagnostic Spectrometer (CDS; Harrison et al. 1995, 1997a) on board the ESA/NASA Solar and Heliospheric Observatory (SOHO).

CDS consists of a telescope feeding a double spectrometer system operating in the extreme ultraviolet (EUV) range from 151–785 Å. We make use of the normal incidence component of the CDS instrument, which maximises the cadence capability. The system disperses the image of a slit (in this case 4x240 arcseconds) onto a 2-dimensional detector, and selected emission lines are transmitted to ground after an exposure. Using a flat scanning mirror one can interleave exposures and mechanism movements to build up rastered images in the selected lines. If one uses the brightest lines, necessary to give the shortest exposure times, and the rastered area is not large, one can obtain image cadences of under 200 s for quiet Sun intensities for areas of several tens of arcseconds square.

All CDS sequences are given acronyms for ease of identification. The sequence used here is called BLINK_ST (blinker 'standard' telemetry rate sequence), and two variations were used, namely variations 10 and 12. The salient details of the two are given in Table 1.

Both variations return data from 6 emission lines, namely He I 584 Å, O III 599 Å, O IV 554 Å, O V 629 Å, Mg IX 368 Å and Mg X 624 Å. The temperatures of formation of these lines are 20,000 K, 100,000 K, 160,000 K, 250,000 K, 1,000,000 K and 1,200,000 K, respectively. This gives data from a good spread of temperature regimes in the quiet Sun atmosphere. As mentioned above, the line selection is dictated by the necessity for bright lines.

As can be seen from Table 1, the slit is rastered across a 40 arcsecond region with a 10 s or 15 s exposure at each location. This takes 151 s or 194 s. Data from the full 240 arcsecond length of the slit are not returned; in variation 10, we just telemeter the central 100 arcseconds, and in variation 12, we return 124 arcseconds. This allows the study of a reasonable portion of the Sun and enables us to reduce the time required to telemeter the data. Since each pixel is 4 arcseconds (east-west) by 1.7 arcseconds (north-south), the resulting arrays, in pixels, are 10x59 and 10x73. In addition, one pixel-width on the detector in the direction of wavelength dispersion represents 0.14 Å in the range 513–633 Å, which covers five of the selected lines, and 0.068 Å in the range 308–381 Å. We choose to select 25 pixels, or bins, of spectral information across the selected emission lines, giving 3.5 Å and 1.7 Å bands in each case.

In each observation run, a piece of quiet Sun was selected and a series of rastered images were made. The details of the 11 runs are given in Table 2.

For each run, the table defines the date and start time, followed by a unique CDS run identification number. The number of rasters in each sequence varies from 60 to 192, giving an observation duration ranging from 3.25 to 8 hours. The pointing information given in the table is given in arcseconds from Sun centre with 'X' positive towards the west, and 'Y' positive towards solar north. The pointings for all of the sequences except those in February 1998 were fixed, that is the Sun's image rotates slowly across the field of view during the observing sequences. The rate at which the Sun rotates through the field depends on the latitude of the target region, but a 40 arcsecond area may rotate through the field in about 4 hours. The February pointings given in Table 2 show the starting location; the value of X increases to follow solar rotation. This is done by stepping the CDS pointing system between rastered images.

Table 1. The BLINK_ST sequence details

Variation	Slit	Raster Area	Exposure	Duration
10	$4'' \times 240''$	$40'' \times 100''$	15 s	194 s
12	$4'' \times 240''$	$40'' \times 124''$	10 s	151 s

3. The sequence of December 4 1997

We now discuss the sequence of December 4, 1997, in some detail to give a representative picture of the entire data-set. The activity identified in this particular dataset is typical of that found throughout.

Fig. 1 shows a selection of images taken through the sequence in the O V line, at 250,000 K. Some 12 images are displayed in time order from top left to bottom right, each image being 40x100 arcseconds in size. The image arrays are 10x59 pixels, but they have been rebinned to 20x59 pixel arrays for the purposes of this display to ensure that the east-west and north-south spatial scales are similar. The full sequence consists of 75 rastered images starting at 15:49:50 UT.

The first feature which one notices is the supergranular structure which is always remarkably clear at these temperatures. Roughly two supergranules can be seen, i.e. the bright network encompasses about two identifiable darker cores. The darker regions are associated with the supergranular upflows and the bright network regions are downflow regions.

A gradual migration of the features can be seen moving to the right of the field of view as the sequence progresses. This is, of course, due to solar rotation, and in the 250 minutes of the sequence the rotation at Sun centre would be of order 40 arcseconds. At the latitude being examined, we see a rotation of order 30 arcseconds.

Clearly identifiable in the sequence, in the network, are well defined, transient bright patches. These appear to lie at network junctions in most, if not all cases – that is, they lie at the sites where three (or more?) supergranules meet. The striking property of these bright patches, which was reported by Harrison (1997a,b), is their transient brightening activity. These 'flashes' are the so-called blinkers. For example, a small blinker can be seen in the right side in the middle of the second frame. It is not bright in the first or third frames. A more substantial event peaks in intensity at the top of frames five and six. A site in mid-frame to the left rotates into the field of view and shows substantial blinker events from frame six to the end of the sequence. A region in the southern portion of the frames shows some brightenings, e.g. in frames 5 and 6 and in the last frame.

This kind of sporadic blinker activity is quite normal. In just a few hours of observation we can identify clearly a reasonable number of events in a small portion of quiet Sun.

Harrison (1997a) identified modest intensity increases of a factor up to 2–3 at the blinker sites. Thus, such events are very

Table 2. The blinker runs

Date	Start Time (UT)	CDS Run	Variation	No of rasters (Duration)	Pointing
22 Nov 97	18h36m11s	9789	10	90 (291m)	X=2,Y=-2
24 Nov 97	12h14m35s	9809	10	60 (194m)	X=1,Y=1
04 Dec 97	15h49m50s	9881	10	75 (242m)	X=-158,Y=281
05 Dec 97	15h49m04s	9892	12	90 (226m)	X=-161,Y=277
06 Dec 97	15h56m36s	9898	12	90 (226m)	X=-160,Y=279
09 Dec 97	17h30m07s	9936	12	110 (277m)	X=-161,Y=-53
03 Feb 98	11h51m57s	10348	12	108 (272m)	X=244,Y=290
04 Feb 98	18h26m23s	10358	12	126 (317m)	X=-162,Y=65
06 Feb 98	05h24m17s	10367	12	192 (483m)	X=-11,Y=15
15 May 98	12h02m37s	11136	12	110 (277m)	X=10,Y=97
18 May 98	13h00m35s	11147	10	105 (340m)	X=0,Y=0

difficult to identify in spatially integrated time-intensity series. Thus, for this study, for each sequence and each bright region, the pixel addresses covering any bright region are identified and the intensity of such a region is examined through the sequence. In cases where there is no compensation for solar rotation, the pixel addresses are updated through the sequence to allow for rotation.

For illustration, we will examine the blinker site which is seen in the northern extreme of the 5th and 6th frame of Fig. 1. A group of 5x5 pixels was identified which covers the site, and its location throughout the sequence projected. As can be seen from Fig. 1, the site is 'quiet' in the early part of the sequence, shows an isolated flash and then quietens again. Fig. 2 shows the spectral bands for this site for an observation before, during and after the blinker event.

The raw data (counts per second per pixel) from the CDS detector have been corrected for several features of the instrument. These include the following. The CCD detector is read out from different quadrants and this introduces a quadrant bias which effectively introduces a background pedestal level which is slightly different for each quadrant. This we remove quite easily by comparing the intensities of non-illuminated regions on the CCD within the four quadrants which are recorded as part of the observation run. In addition, the microchannel plates (MCP) used in the detectors degrade with accumulated charge (effectively with time). Given the fact that the spectrum is fixed on the CDS detectors, this results in a 'burn-in' at the locations of the lines. This is corrected for using a flat-field technique which makes use of a regular narrow-wide slit comparison monitoring programme. Finally, we take acount of the calibration of the NIS spectra to convert to units of photons/sec.

The final intensity carries an absolute error which may be of order 30%, but it is the relative intensities and their variations which are of interest in this work in which case we must consider errors which are much less than this.

Let us examine the wavelength windows of Fig. 2, to confirm the identification of the lines listed in the table above. In each panel, the solid profile shows the emission during the blinker event (image 27), the dashed curve shows the pre-blinker emission (image 20) and the dash-dot curve shows the post-blinker emission (image 41). For quiet Sun spectral identifications the reader is referred to Brooks et al. (1999).

The He I band (top left) contains data from 582.9 to 585.7 Å and this band is dominated by only one line, the He I line at 584.33 Å.

The O III band (top right) runs from 598.1 to 600.9 and contains only the O III line at 599.6 Å.

The O IV band is a little more complex, running from 553.1 to 555.9 Å and containing an O IV multiplet. The main line is at 554.5 Å, but we expect some contribution from the lines at 554.076 Å, 553.329 Å and 555.263 Å. These three lines do not show as clear peaks, but their intensities serve to raise the apparent background and alter the shape of the main O IV curve. Having said that, we should stress that all of these lines are from O IV; there is no 'contamination' from a second ion.

The O V band (middle right) contains data from 628.3 to 631.2 Å and is dominated by the lone and very strong O V line at 629.73 Å.

The Mg IX band (bottom left) runs from 367.2 to 368.9 Å and, although it is dominated by the bright Mg IX line at 368.07 Å, there are weak Mg VII lines at 367.67 and 367.68 Å.

Finally, the Mg X band (bottom right) which runs from 623.5 to 626.3 Å is dominated by the Mg X line at 624.94 Å but does contain the lines O IV at 624.62 Å, Si X at 624.73 Å and O IV at 625.13 Å. These lines cannot be identified in the plot, though their contributions may influence the Mg X curve.

In effect, we have six wavelength bands which are each dominated by one line or ion of interest. Comparing the three curves from each band, for this event, the oxygen lines show a clear increase in intensity during the blinker event, the helium shows a marginal increase, and the magnesium lines either remain level or even show a slight decrease in intensity.

In Fig. 3, we plot the time-intensity curves for the six bands for the 4 December period, for the 25 pixel group (summed). We do not fit the lines or remove background because the emission in each wavelength window is dominated by the emission line of interest (Fig. 2). Any trends in line intensities, ratios etc... should be clearly visible. The start time of the plot is given in Table 2. For the display here, we simply give an abscissa in seconds of elapsed time.

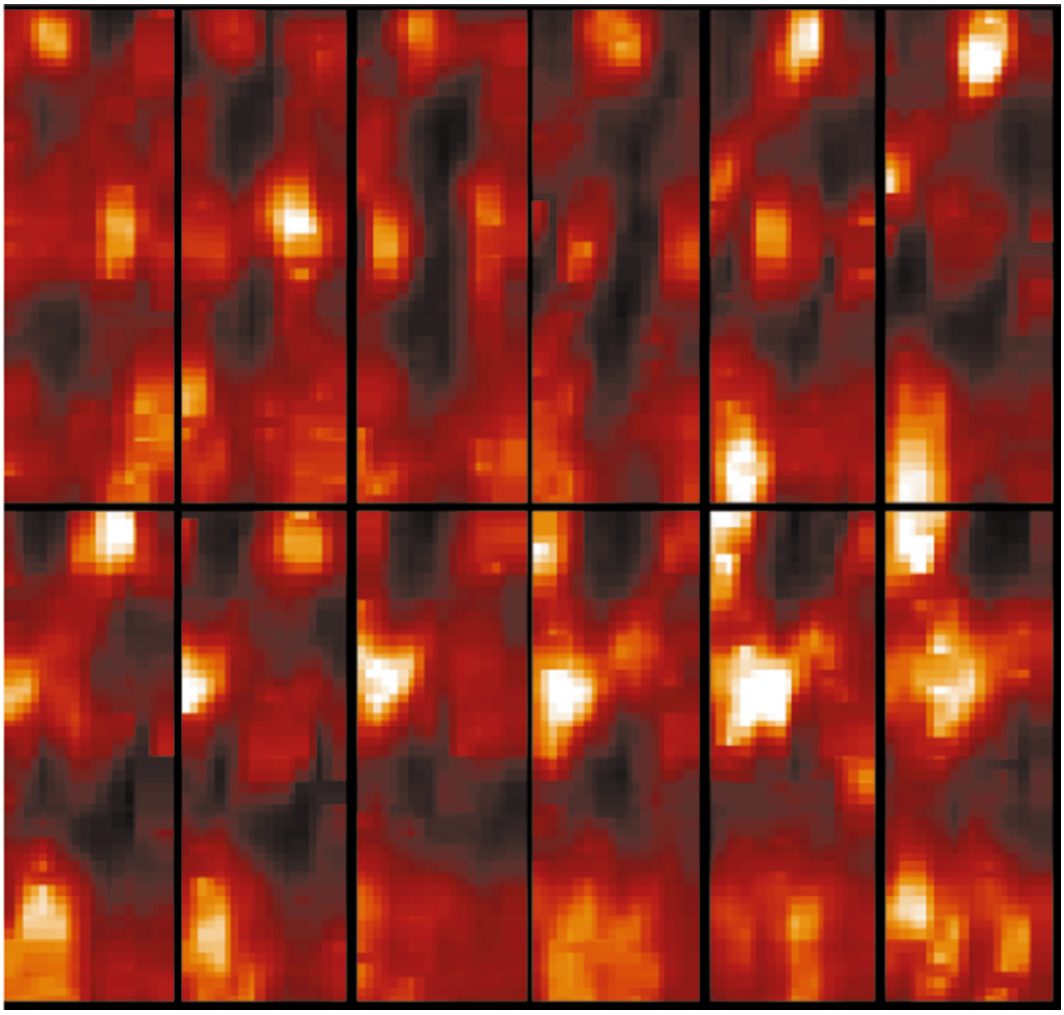

Fig. 1. A sequence of images of a quiet Sun region on December 4 1997 in O V 629 Å with time running from top left to bottom right. The figure shows selected images from a 75 image sequence, with images at 16:16:47 (image 8 of sequence), 16:33:39 (image 13), 16:43:45 (image 16), 16:57:14 (image 20), 17:24:11 (image 28), 17:44:21 (image 34), 18:04:31 (image 40), 18:55:12 (image 55), 19:12:06 (image 60), 19:28:54 (image 65), 19:39:02 (image 68) and 19:52:29 (image 72).

Much variability can be seen, typically at the 10–20 percent level, depending on the emission line in question. However, in all lines we see a significant brightening – the blinker – which starts some 4–5000 s into the run and lasts for approximately 2000 s. The blinker appears to have 2–3 peaks but this may be the intrinsic solar variability superimposed on a more significant intensity increase of the blinker. The increase in intensity is of order a factor of 2 for the three oxygen lines. It is much less for the hotter (Mg) and cooler (He) lines, which rise by a factor of about 1.2 to 1.3.

In many ways, this is a typical blinker event, being an isolated brightening which is most apparent in what we think of as transition region temperatures. Perhaps less typical is the fact that this event is visible to some extent in all lines.

It should be noted that because of the solar rotation, the projected path of the 25 pixel group which defines the blinker site actually starts to leave the western edge of the field of view from 13,000 s into the sequence. Hence the rapid decline at the end of the observation.

The rotation rate of all of the sequences is estimated by comparisons of the supergranular patterns through the sequence. This is a crude approach, but the pixel groups chosen to cover the bright blinker sites are larger than the blinkers themselves so there should be no loss of intensity due to a blinker site moving out of the pixel group being tracked.

In order to investigate any temperature and density effects we plot in Fig. 4 the ratios of the intensity curves of Fig. 3. Remember that the blinker event peaked at about 5500 s into the sequence. Also, note that the rapid changes in the ratios at the end of the sequences are due to the loss of intensity towards the end of the sequence (14500 s onwards), and should be ignored.

All of the emission lines used are from allowed transitions and so their intensities will respond to density changes in the same way, i.e. their ratios would show no significant variation to a pure density ‘event’. We do note, however, that the He I

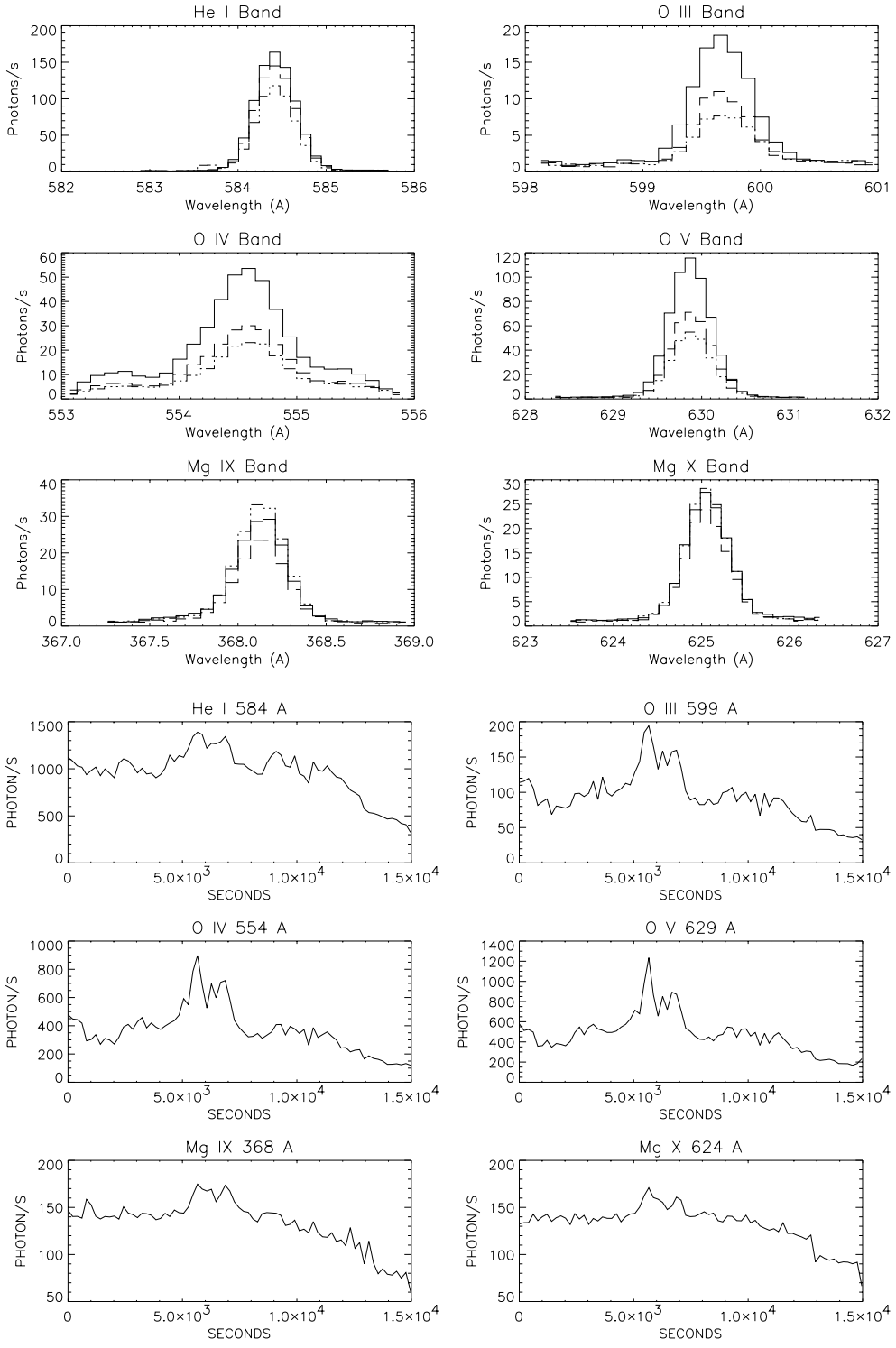

Fig. 2. The six wavelength bands used in the blinker analysis, centred on the lines He I 584 Å, O III 599 Å, O IV 554 Å, O V 629 Å, Mg IX 368 Å, Mg X 625 Å. Three curves are shown for each, for the pre-event (dashed), event (solid) and post-event (dash-dot) phase for a blinker on 4 December 1997. This is a 75 raster run (Table 2), and the spectra are taken from a sum of the 5x5 pixels for the rastered images 20, 27 and 41.

Fig. 3. A blinker event displayed in all six wavelength bands. We plot the time-intensity curves for a 25 pixel group on 4 December 1997 covering the blinker shown at the top of frames 5 and 6 of Fig. 1.

line is optically thick (Brooks et al. 1999) and that its intensity may be influenced by excitation from coronal radiation. For this reason, the He I line is not the ideal 'cool' line to use. However, given the need to use bright lines for this particular study, it is the only realistic line to use with a characteristic temperature below 100,000 K.

Considering the intensity ratios of Fig. 4, the lack of any clear change in the ratios of the oxygen pairs across the period of the blinker event is quite remarkable. Despite factors of about 2 increase in intensity, the oxygen line ratios remain stable. The three lines used have characteristic temperatures of 100,000 K, 160,000 K and 250,000 K. Thus, their ratios might be expected to vary if there had been a significant change in temperature. The lack of a change suggests that the increase in emission measure which characterises the blinker is due predominantly to an increase in density and/or filling factor, and this is most

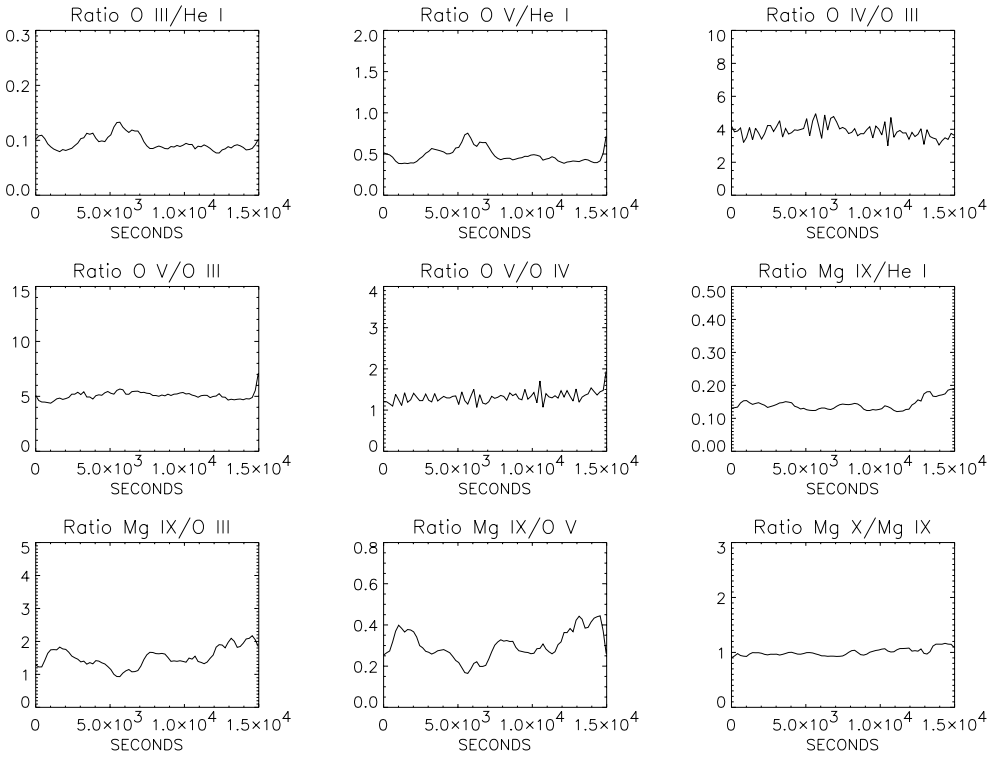

Fig. 4. For the same period and pixel group used in Fig. 3, the ratios of the intensities of the various emission lines are plotted. The behaviour of these ratios can be used to determine temperature and density variations.

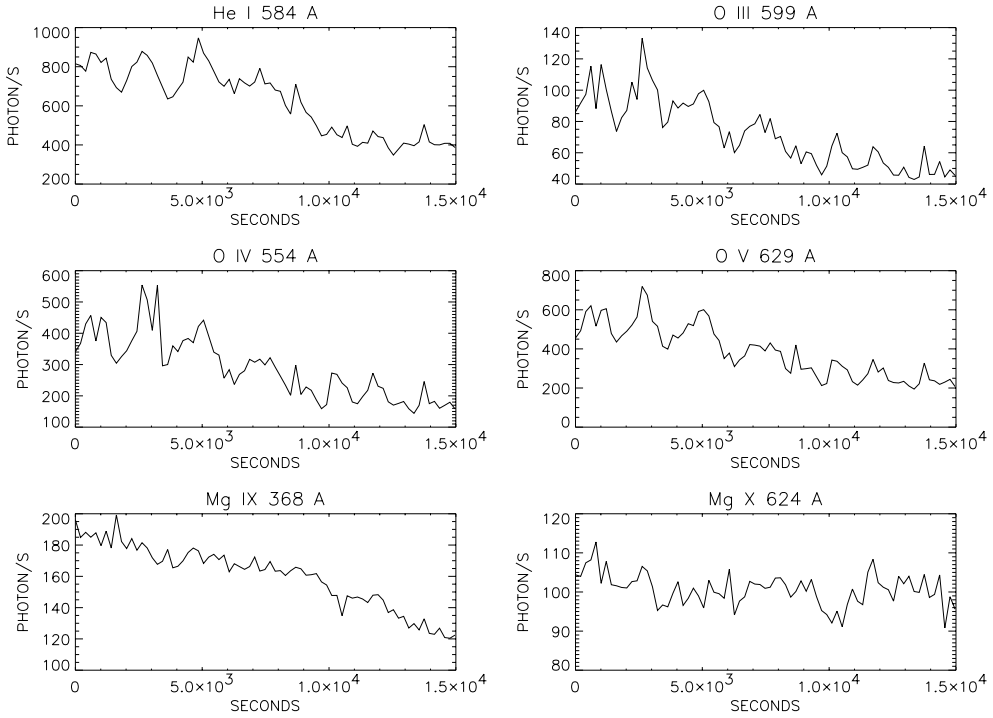

Fig. 5. An example of repetitive blinker actvity from one region on December 4 1997

evident in the transition region temperature plasmas. There is some evidence for heating, for example in the signatures of the Mg lines, and this suggests that we may be witnessing a density or filling factor enhancement in a cooling plasma. We discuss this further in a later section.

However, this is an inspection of only one blinker event and should be compared to the analysis of the full data-set later on. Having said that, it is typical in many ways.

For an illustration of a rather different form of blinker activity, we now look at the small bright core which displays a bright blinker in the centre of the second frame of Fig. 1.

The intensity-time curves for the six emission lines are given in Fig. 5, in a similar display to Fig. 2. This is for a group of 3x6 pixels which cover the blinker region, which track from the extreme left (east) of the image at the start of the sequence, and just reaches the right hand (western) side at the end of the sequence.

The region shows a slow decline in intensity but, superimposed on the decline, is an almost regular set of blinkers occurring at about 2000 second intervals. The peaks are very clear in all oxygen lines and in the He I, on this occasion. They are not evident in the Mg IX curve and there may be weak, though not compelling evidence for the peaks in the Mg X curve. This could possibly be a signal of the O IV lines mentioned above, which are expected to contribute under 10% of the intensity of the band.

Regular blinker activity is of great interest because of its potential for identifying periodic activity in, for example, the supergranular cells – possibly leading to estimates of plasma flow speeds in the cells, cycle times etc... However, this is an unusual event and an analysis of blinker regularity is given later. Nevertheless, this single event sequence may provide useful information.

The top panel of Fig. 6 shows the O V intensity curve of Fig. 5 (mid-right panel). To analyse the variability, the slowly varying (declining) component has been removed, using a linear function running from 450 photons/s to 175 photons/s through the sequence. The curve has also been smoothed, using a 3 bin boxcar method. For comparison, a sine curve of period 1940 s (10 $\times$ the raster cadence), peak to trough of 200 and an average of 100 is produced. Clearly this provides a fair mimic of the actual variability for portions of the sequence.

The lower panel of Fig. 6 shows an autocorrelation of the two curves plotted against raster number through the sequence. The sine curve produces clear, equal peaks at 0, 10, 20, 30 and 40 rasters, where 10 rasters is equal to 1940 s. The actual data show significant peaks at 0, 10.5 and 21.0 and a broad peak at 32 to 38, i.e. 0, 2037, 4074 and 6208 to 7372 s, respectively. This indicates a periodicity of about 2037 s, with a secondary contribution at 6000–7000 s mainly due to the broad peaks in Fig. 6 between 6500 to 9000 s and after 11000 s into the sequence.

It is concluded that there is a quasi-periodic activity taking place but its importance should be considered in the light of the analysis of the complete data-set.

The basic analysis presented of the events of December 4 has served as an illustration of the nature of the blinker activity which is to be analysed statistically in the next section.

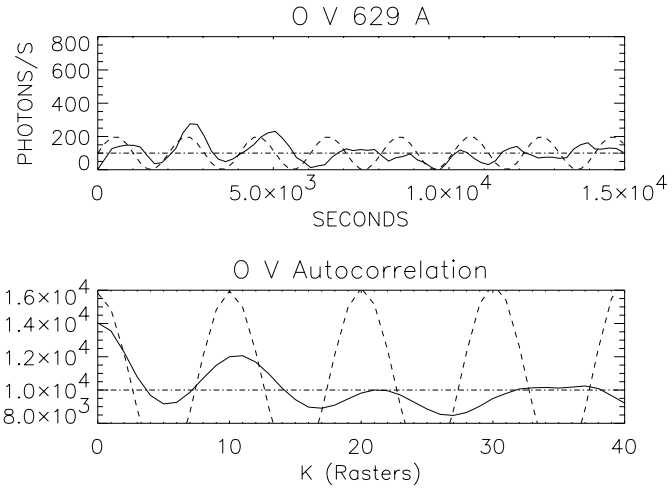

Fig. 6. Top: The O V intensity curve for the blinker series of Fig. 5, smoothed and with a slowly varying background removed. A sine curve is shown for comparison. Bottom: An autocorrelation of the curves of the top panel.

4. A statistical analysis

Having described features of the 4 December 1997 events to illustrate blinker activity, we now turn to a statistical analysis of blinker activity for the entire set of 11 observation runs.

Each of the blinker runs listed in Table 2 have been inspected visually. The principal sites of brightenings for each sequence have been identified using the O V observations, and in every case the pixel addresses of the sites have been noted. We use the O V data to locate blinker activity because it displays the greatest increases in intensity. In this first stage we use a visual approach simply to define the pixel groups of interest; a calculation of the precise intensity variations in the pixel groups comes later.

For each blinker pixel group identified, we wish to examine the detailed intensity profile of that group. In each case, compensation for solar rotation is included, to ensure that the intensity profiles are not influenced by intensities crossing out of the defined pixel regions. Thus, for each site the intensity curves in each wavelength band have been produced and this forms the basis of the analysis of this section. A code has been written which takes the pre-defined pixel group, including the solar rotation compensation, and extracts the time-intensity curves for each group. Initially the time-intensity curve is smoothed to reduce noise. The code then steps through the O V intensity curve searching for intensity 'events'. Any method selected for such an exercise will be somewhat arbitrary and must cater for intrinsic scatter or remaining noise. We have chosen to define an event onset when the O V intensity of the pixel group rises at least 10% above the average of the last three measurements (rasters). Comparing to the average of three measurements excludes some increases which are simply due to noise. Once an event onset is noted in this way, the code continues through the intensity curve and notes the peak intensity value and time, and the end time of the event. The end time is defined as the time when the intensity drops again to within 10% of the pre-event intensity.

Finally, the pre-event intensity count-rate and event peak intensity count-rate are compared. The event is only retained if the difference is greater than the square root of the pre-event intensity count-rate.

It should be noted that events which are truncated at the end of observing periods are not counted unless their intensities have returned to the pre-defined intensity level. In addition, events

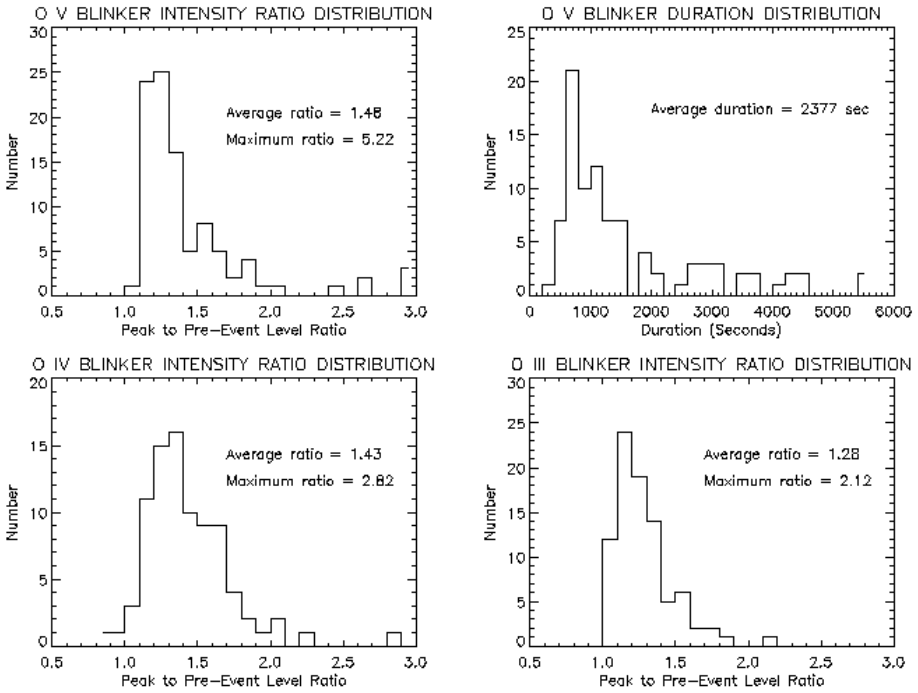

Fig. 7. Analysis of the oxygen intensity profiles for the blinker data-set. The top left panel shows the distribution of the O V peak to pre-event intensity ratio. The top right panel shows the distribution of O V event durations. The bottom two panels show the peak to pre-event intensity ratios for the O IV and O III data. The expected error bars are of order the square root of the count for any particular bin.

which may be underway at the start of observing runs are not counted.

In this way, for the 11 quiet Sun observations, and the identified sites of brightenings within those observations, we have identified a large number of brightenings using the O V data. In all, we found 97 blinker events and for each we have noted the pre-event, peak and post-event intensities in all 6 lines, as well as the event onset, peak and end times, and event location.

The criteria used to identify a blinker event, e.g. the intensity increase necessary to include an event, and the definition of the end-time, are such that some events may not be counted, for example, events superimposed on a rising intensity background. Visual inspections of the profiles suggest that this is not common, and it is hoped that the resulting blinker data-set in any case can be used to explore the physics of blinker activity even if some events are overlooked.

4.1. Intensity profiles

Fig. 7 shows the properties of the blinker events detected in the oxygen data. Three panels show the distributions of blinker intensity increases, i.e. the ratio of the blinker peak intensity to the pre-event intensity, for O III, O IV and O V. The top-right panel shows the distribution of durations of the O V events.

The peak to pre-event intensity ratio in O V varies from 1.08 to 5.22. The distribution has a clear peak, with 67% of the events lying in the range 1.10 to 1.39. The average intensity increase is 1.48. The drop of the distribution at under 1.10 is due to the fact that weaker events were rejected on the grounds of statistical significance, and the code did not identify intensity increases of less than 10%. This being the case, we must conclude that the curve may remain high, or even show a significant rise to lower values. However, the 1.10–1.19 bin does display a slightly lower value than the 1.20–1.29 bin, suggesting that the curve may be falling. Of course, we were not scanning the data for intensity events of less than 1.0 so these would not appear in the curve of Fig. 7. However, even with these restrictions it is clear that there are a high number of brightenings and that the most common intensity increases are less than a factor of 1.39 above the pre-event intensity.

The duration of the O V events shows a spread from just a few hundred seconds to several thousand seconds. The bulk of the events (66%) lie in the range 400–1600 s, yet the average duration is 2377 s, mainly due to a tail of long-duration events. The selection method used in the code does not allow the event onset and end times to be in adjacent rasters, so the shortest duration an event can have is 302 s and 388 s for variations 10 and 12, i.e. twice the time between two rasters. Thus, we cannot draw any conclusions about events of durations less than this, beyond stating that the distribution does indicate a fall below 600 s.

One important feature to establish immediately is the comparison of blinker durations to anticipated cooling times. Are these events simply the result of one heating ‘event’ after which the plasma cools? Typical cooling times for such plasmas at typical transition region densities and O V temperatures are in the region of just a few seconds to a few tens of seconds, depending on the actual density used and the temperature. Higher temperature plasmas at, say, 1 million K and typical coronal densities may have cooling times of approaching 1000 s. Given these figures and the predominence of transition region temperatures, we can state that the blinker events are driven by activity which most likely continues to dump energy into the plasma throughout the blinker duration – there is a continuous energy input through the event.

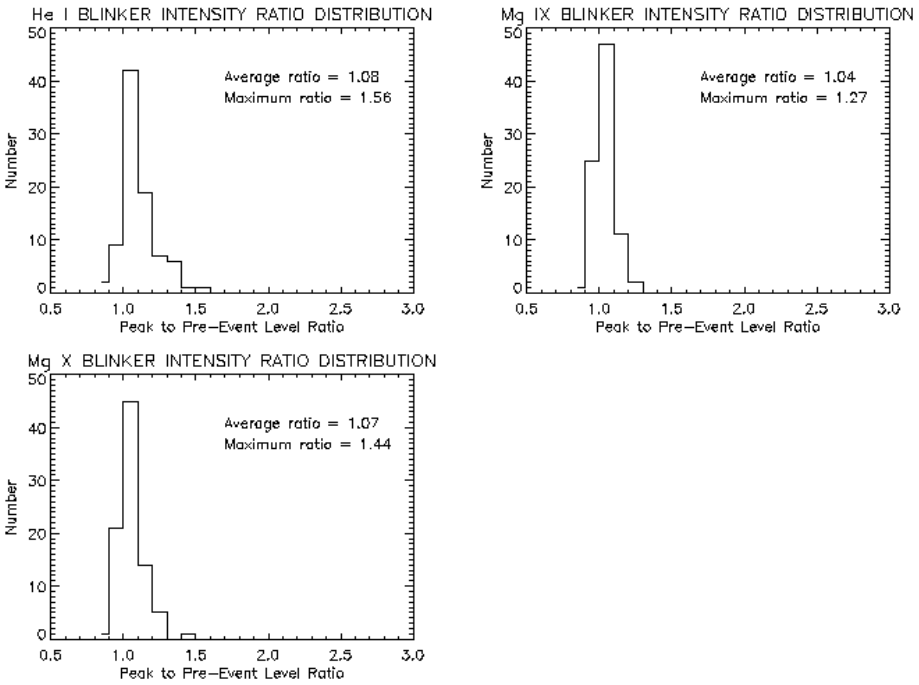

Fig. 8. Blinker peak to pre-event intensity distributions similar to the oxygen distributions of Fig. 7, for the helium and magnesium data. The expected error bars are of order the square root of the count for any particular bin.

Fig. 7 also shows that the average intensity increase for the O IV events was 1.43 and for O III was 1.28. Both show smaller increases on average than the O V events, though the O IV and O V increases cannot be considered to be significantly different. The O IV increases generally show a more variable increase, displayed as a wider peak in Fig. 7 (72% of the events in the range 1.10 to 1.69). The O III curve has a similar width to the O V distribution (with 71% in the 1.0 to 1.39 range). The O IV curve shows a significant fall off to values less than 1.2. Indeed, this curve also shows a value at less than 1.00, i.e. for one identified brightening in O V there is a drop in intensity in O IV, albeit a weak one.

Fig. 8 shows the same data for the helium and magnesium lines. The average He I increase is only 1.08, with a maximum increase of 1.56 and 63% in the range 1.0 to 1.19. Note that many events effectively see no blinker when the O V curve blinkers are identified, and some show a slight negative intensity change – which is most likely due to normal variability. The Mg X and Mg IX data show equally narrow distributions with average increases of 1.04 and 1.07 and, again, some events at less than 1.00.

Thus, the average blinker shows the following characteristics: an increase in intensity of 1.08 for He I, 1.28 for O III, 1.43 for O IV, 1.48 for O V, 1.04 for Mg IX and 1.07 for Mg X. The average duration is 40 minutes. However, these averages are influenced by rather extended tails to the distributions. Thus, for the purposes of discussing a 'typical' blinker it is better to use the following characteristics, based on the peak values in Figs. 7 and 8: duration 1000 s (17 min), intensity increases of 1.05 for He I, 1.2 for O III, 1.4 for O IV, 1.3 for O V, 1.05 for Mg IX and 1.05 for Mg X.

4.2. Line ratios

Throughout the blinker events in the 4 December 1997 observation (Sect. 3) there was no significant variation in the O V, O IV and O III emission line ratios. This was used to suggest that we are observing a density enhancement. This property is common to the blinker data-set and we show this by displaying a set of examples in Figs. 9 to 11 and examining a scatter plot of the entire data-set.

Fig. 9 shows the O V intensity profile for a blinker event on 22 November 1997. Despite an intensity increase of near a factor of 2, the O IV/O III, O V/O III and O V/O IV ratios remain fairly static at about 4.0, 5.5 and 1.3. These values are remarkably similar to those given for the event discussed in Sect. 3. There is a marginal increase in the ratios, especially for the O V/O III ratio at about the time of the blinker, but it is certainly less than a factor of 1.2. We are seeing essentially the same picture.

The line ratios are remarkably similar, again, for the 4 December 1997 blinker shown in Fig. 10 (this is not the event discussed in Sect. 3) and the 18 May 1998 event shown in Fig. 11.

Fig. 12 shows the relative O V and O III intensity increases for the entire blinker data-set as a scatter plot. Each data point represents one blinker event and represents the ratio of the O V peak intensity to pre-event background intensity plotted against the ratio of the O III peak intensity to pre-event background intensity. The solid curve shows the curve for which the O V and O III relative increases would be equal, i.e. an increase of a certain magnitude above the background or pre-event level is the same in the two lines. We know that the data-set does not adhere strictly to this line since the distributions of intensity increases shown in Fig. 7 are not identical; the O III line on average shows a weaker increase than the O V line. However,

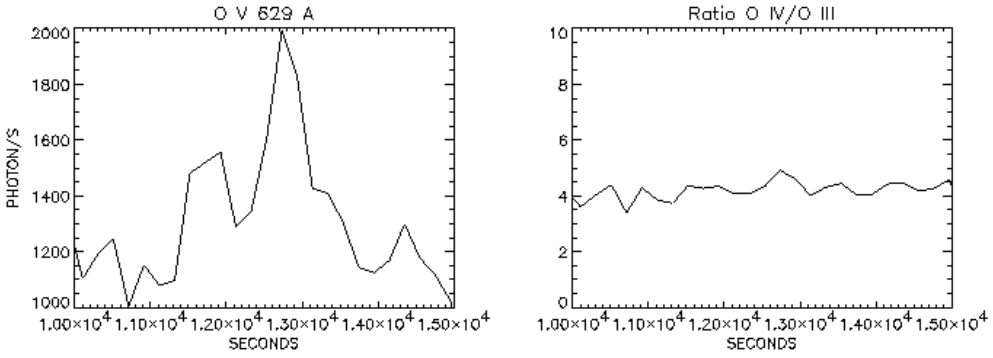

Fig. 9. A blinker recorded on 22 November 1997 in O V. The intensity of the O V line plotted against time from the start of the observation run is shown in the top left panel. For the same time period, the remaining three panels show the ratios of the O IV/III, O V/O III and O V/O IV intensities. No significant increases or decreases are detected during the blinker event.

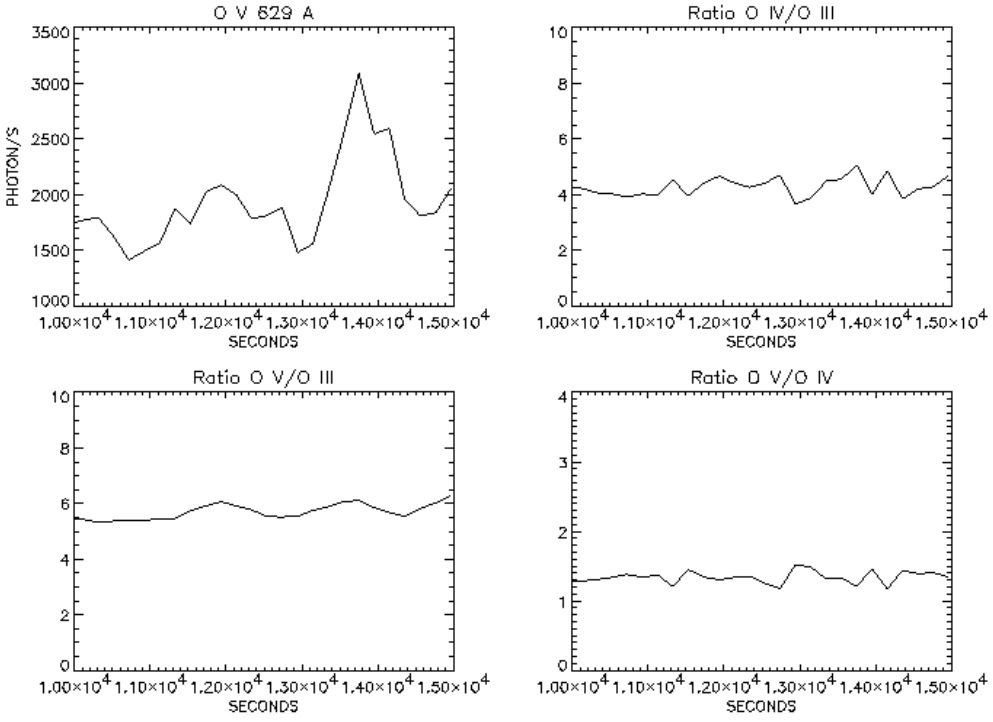

Fig. 10. A blinker recorded on 4 December 1997 in O V. See caption for Fig. 9 for explanation of format.

the scatter plot does show a linear distribution which is pretty neatly distributed about the dashed line, represented by I_{OV} = 1.11 I_{OIII} – 0.055, where I_{OV} is the intensity increase for the O V line. Most events cluster in the 1.0 to 1.4 region in both O V and O III and in this region the two curves shown in Fig. 12 are very close to one another. Thus, for most events there is no significant variation in the O V to O III intensity ratio detected.

Thus, it seems that the lack of a significant change in the oxygen emission line intensity ratios is a common characteristic of the blinker events and, again, we conclude that this points to an event type which is predominantly a density or filling factor enhancement.

4.3. Blinker thermal energy content

One simple way of estimating the energy content of a blinker event is to compare the non-event emission measure to the event emission measure, in order to take into account the effects at all

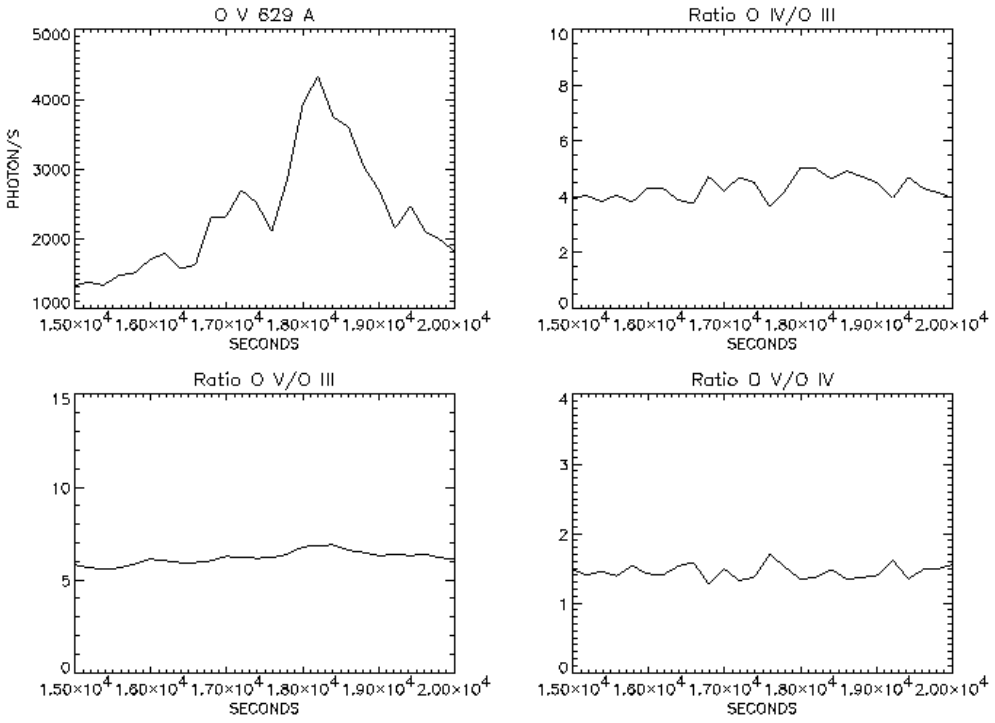

Fig. 11. A blinker recorded on 18 May 1998 in O V. See caption for Fig. 9 for explanation of format.

temperatures. Thus, to calculate the total thermal energy content of a typical blinker event we first take the emission measure values corresponding to the formation temperatures of He I, O III, O IV, O V and Mg X using the emission measure distribution due to Raymond and Doyle (1981). They define a column emission measure as the differential emission measure integrated over 0.1 in $\log T_e$ around the temperature of maximum abundance of the emitting ion. We converted their values to volume emission measures using a typical blinker area of 5x5 pixels i.e. about 5.5 $\times$ 10^{17} cm^2. We also took an additional point at $\log T_e = 5.7$ which brings the integrated emission measure value to within 2% of the result using the full curve. We introduce also a filling factor to account for the actual volume of the blinker. Thus our emission measure curve uses values defined as

$$\int_{V_{obs}} N_e^2 f dV_{obs} \quad (1)$$

where V_{obs} is the observed volume of the blinker (limited by the CDS resolution), N_e is the electron density and f is the filling factor.

In practice, for this calculation, we used a filling factor of 1. The filling factor is noted explicitly in the definition to make the mass and energy dependence on f apparent. We then integrated the curve in temperature to obtain a total volume emission measure of 6.1×10^{49} cm^{-3} and multiplied by Boltzmann's constant (k) to derive an energy density;

$$k \int_T \int_{V_obs} N_e^2 f dV_{obs} \quad (2)$$

From this calculation we obtained a value of 8.43 $\times$ 10^{33} cm^{-3} erg.

For the moment, let us consider the average blinker event. We adjusted the five points corresponding to the emission lines

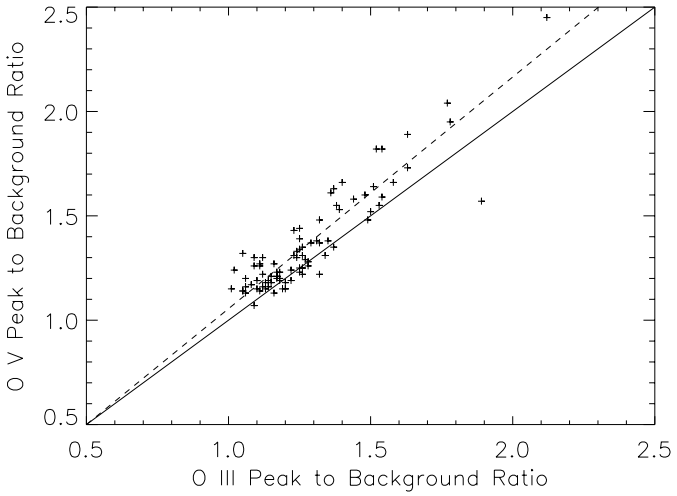

Fig. 12. A scatter plot indicating the relative intensity increases in the O V and O III lines for the entire blinker data-set. For each event (indicated by one data point), the ratio of the O V peak intensity to pre-event background intensity is plotted against the ratio of the O III peak intensity to pre-event background intensity.

by the average increases given in Figs. 7 and 8, i.e. 1.08 for He I, 1.28 for O III, 1.43 for O IV, 1.48 for O V and 1.07 for Mg X. We repeated the integration to obtain a value of 6.56 $\times$ 10^{49} cm^{-3} for the total volume emission measure and 9.05 $\times$ 10^{33} cm^{-3} erg for the energy density. Thus we can identify the difference as the total volume emission measure and energy density contained in the blinker ($\sim 4.5 \times 10^{48}$ cm^{-3} and ~ 6.3 $\times$ 10^{32} cm^{-3} erg, respectively).

The desire is to make an order of magnitude estimate, to assess the potential impact on the coronal plasmas and gauge

the importance of these events in the global picture. For this reason, at this stage, we do not repeat the calculation for every event, but consider only this average blinker.

We may obtain a total thermal energy by dividing the energy density by a density estimate. If we assume a typical transition region density, say 10^{10} cm^{-3} we find that we require an energy of 6.3×10^{22} erg to produce the average increases found. However, this would produce one pulse which mimics the intensity increases detected but decaying rapidly with a cooling time of order, say, 10 s. To maintain these intensities, we can consider a series of such energy pulses. Considering the cooling time and placing each new pulse some 7 s after the last, one can integrate the effects from each pulse and thus maintain the intensity peak required. This is rather crude, but given our lack of knowledge of the cooling time (Sect. 4.1), it is sufficient for an order of magnitude estimate of the total blinker thermal energy content. We find a total energy for our average blinker event of 2.1×10^{25} erg. This is very near to the estimated thermal energy of 4.4×10^{25} erg calculated by Harrison (1997a,b), and is of order a few times 10^6 less than the energy content accepted for a typical flare. Thus, in terms of energy content, the blinker can be defined as a micro-flare.

We noted in Sect. 4.1 that the average blinker characteristics may not be the best figures to use. In fact, it is the duration which has the greatest influence in the energy calculation since the long-duration tail of the top-right panel of Fig. 7 produces an average a factor of two greater than the mode. This suggests that our more common blinker duration of, say, 1000 s would contain approximately 10^{25} erg in thermal energy.

The estimated energy is of course dependent on a number of factors. Assuming the blinker occupies all of the 5x5 pixel area and assuming a depth of 1000 km we can estimate the electron density from the total volume emission measure as $\sim 2.9 \times 10^{11}$ cm^{-3}. Using this density instead of the typical transition region density results in a total energy a factor of 30 lower. If the density remains the same but the filling factor is lower the emission measure (and hence energy) will also be lower. More precisely, a maximum filling factor (1) and a typical transition region density (a lower limit) should give us an upper limit to the total energy of the blinker. Of course, we note that a low filling factor and high electron density could give us the same emission measure as derived here. The energy itself is proportional to the density and the square root of the filling factor ($E = nkT \equiv N_e f V_{obs} kT$) and hence the density is also proportional to the inverse of the square root of the filling factor.

In the next section we consider blinker rates, but, taking the result from that section, there may be 3,000 blinkers in progress on the entire solar surface at any point in time. Thus, we find a total energy release rate per area of the entire solar surface at about 10^3 erg s^{-1} cm^{-2} which is over two orders of magnitude less than the radiative loss of the upper chromosphere and corona as estimated by Athay and White (1978) (6×10^5 erg s^{-1} cm^{-2}). Thus, even though there may be many short-duration blinker events undetected by the present study, it seems certain that the thermal energy from the blinkers is not sufficient to power the heating of the corona, which should be no surprise given the lack of observed high temperatures and the modest increases in intensity.

Indeed, it has to be stressed that it is purely the thermal energy content that has been calculated and it tells us nothing, for example, about the kinetic energy in any accelerated plasma, the energy carried in any waves propagating from the blinker site, and the energy in plasmas at temperatures not sampled by the emission lines being used. Although it is less than that required to heat the corona, this should not be taken to mean that the blinker events have no role in coronal heating. This would be assuming too simplistic a picture.

4.4. Blinker frequency and sympathetic blinkers

Given the fact that we recorded 97 events in the 188,746 seconds of observation using the CDS rasters of areas given in Table 1, we can estimate the frequency and number of blinkers for the entire solar surface. From the observations, we recorded about 2×10^{-13} event onsets per km^2 per sec. The solar surface is 6.2×10^{12} km^2. Thus, the observations suggest the onset of 1.24 events per second over the entire solar surface. This does assume that the occurrence in coronal holes and active regions is similar to the quiet Sun, but it provides a useful order of magnitude. Given the average duration, at any moment in time there may be 3,000 blinkers in progress over the entire disc.

Using this set of 97 blinkers, we can explore several other questions. For example, when a blinker occurs, what is the average time to the next event, and is it most likely to occur in the same site, or elsewhere?

Some of the blinkers in the data-set were coincident in time but from different locations within the field of view. In addition, we cannot state the site of blinkers which precede the first blinkers identified in each data run. Thus, we have 79 occasions where we can compare the blinker site to the site of the following recorded blinker. We must remember that we are viewing an area of only 40×100 arcseconds or 40×120 arcseconds at a time. Blinker sites rotate out of the field of view and adjacent sites may be out of the field. However, a comparison of blinker onset occurrence in the sites we can view still provides an astounding result. Of the 79 occasions where we can compare the blinker site to the following blinker site we find that in 85% (67 events) of the cases, the blinker onset occurs at a different site to the last blinker onset. In only 15% (12 events) of cases was the next blinker onset from the same site. Despite the limited field of view in these observations, these appear to be very significant findings.

This result could mean one or more of three things: (i) the site which is active has released stored energy and some build up is required for the next blinker, thus a non-blinking site is more likely to produce a blinker next; (ii) the blinker activity is sympathetic, i.e. a blinker can trigger a blinker at a remote site; (iii) the blinker rate is so great that the next blinker in a given area is likely to occur before the blinker at the first site is finished.

To explore this further, we ask what the average time is from a blinker onset to the next blinker onset. Again, for the 79 cases

Table 3. A summary of the delay between a blinker event onset and the next blinker onset from the same site

Delay Time Between Onsets	No of Events	Percent of Cases
under 1000 s	3	5%
1000–1999 s	17	28%
2000–2999 s	14	23%
3000–4999 s	11	18%
5000–6999 s	5	8%
7000–8999 s	7	11%
over 9000 s	4	7%

we can show that this time is 1494 s, with 65% at less than 1500 s, 73% at less than 2000 s, and 84% at less than 2500. Remember that the average blinker duration was 2377 s, with most blinkers in the range 400–1600 s. Given the average duration and the average time between blinker onsets we can only conclude that option (iii), above, is true, i.e. from the data we have there is no evidence for sympatheic blinker activity.

We can also ask how long it is from a blinker event to the next blinker event from the same site. This may give a measure of the time required for a region to 'recover' from the first event, or it may tell us something about any periodic behaviour associated with the driving activity, such as convection cell flows.

From the data-set, we have 61 cases where we can specify how long it took for a specific blinker site to display a blinker again, i.e. we detected a blinker following an earlier blinker at the same location. The distribution of times is shown in Table 3. We note that in over 50% of cases the next blinker occurs at the same site in the period 1000–2999 s. Delays of under 1000 s are rare, but this may be subject to the limitations of the detection method.

There is no strong peak which would be consistent with a common periodic behaviour such as that shown for the December events in Fig. 5. Indeed, to summarise: after a blinker event onset there is a 50% chance of a further blinker onset from the same site in under 3000 s, but there is a 73% chance of a blinker onset from another site close by within 2000 s.

5. Modelling the blinker intensity signatures

Using the Arnaud and Rothenflug (1985) ionisation balance calculations modified for electron density effects as implemented in the Atomic Data and Analysis Structure atomic database and codes (ADAS – originally developed by the JET Joint Undertaking, see Summers, 1994) we have been able to calculate the expected line ratios over the pressure range (electron density x temperature) 10^{14} to 10^{18} cm^{-3} K.

The emission measure adopted to account for ratios between ionisation stages was that of Raymond and Doyle (1981). We adopted the coronal abundances of Feldman (1992) for ratios between different elements.

It is interesting to note that for all three oxygen/oxygen ratios shown in Fig. 4, the calculated ratios are significantly higher than those observed, for all of the pressures considered. For example, for the O IV/O III ratio the ADAS calculation gives a ratio of about 8.0 at lower pressures, falling to 6.4 above 10^{16} cm^{-3} K, which compares to the observed value of 4.0 $\pm$0.75. The O V/O III and O V/O IV ratios are similarly much less than the calculated values.

If the ratios are correct and the ADAS calculation is correct then the implication is that we have extremely high pressures, at least two orders of magnitude greater than expected. This is very unlikely. The mismatch between observation and theory/calculation may be due to instrument calibration, or it may require a reassessment of the atomic calculations and/or the physical assumptions (e.g. a non-Maxwellian plasma). The calibration and application of atomic calculations have been applied to the best of our abilities at this time and the result, here, will be used to assess the methods used and the assumptions adopted. It is interesting to note that predicted intensities from the 'Chianti' atomic data-base (see Dere et al. 1997) also suggest that the ratios represent extremely high pressures. With regard to calibration, we believe that the CDS-NIS calibration is good to 20–30% for the bright lines used in this work, and would thus not expect the CDS calibration to be responsible for the mismatch between observation and calculation.

The saving feature here is the fact that we can draw two conclusions from the lack of a ratio signal for the blinker in the oxygen data, without the need for an absolute ratio calculation. Firstly, the intensities should vary equally with density since these are allowed transitions – and we do see an equal variation. Secondly, if there was an increase (or decrease) in temperature, one would expect to see evidence through a change in the ratio; such a variation is not seen.

Similar problems exist in calculating the expected ratios for the ratios involving He and Mg in Fig. 4. Of course, it is possible that we are observing an event type which is so restricted in its location that its influence is confined to the so-called transition region temperatures of a few hundred thousand K. In this case, ratios with the hotter and cooler lines are not meaningful since their colocation is simply due to a line of sight effect. However, we are still faced with the fact that the oxygen ratios, which come from similar temperatures also had the inconsistency. For this reason, at least part of the problem must relate to the atomic calculation assumptions and, specifically, the ionisation balance.

The ratio of line intensities from different ions depends critically on the ionization. The observation that the O V, O IV and O III line ratios retain the average quiet Sun ratio inspite of there being a sudden brightening in the lines by a factor three implies that the blinker oxygen emitting plasma has the same ionization as the quiet Sun. Any model to explain the observed ratio must therefore be insensitive to initial conditions and should not assume either energy or ionization balance as an initial condition.

In order to progress in the interpretation of line ratios, we therefore require a time-dependent model. The observed lines are emitted in the temperature range 10^5–10^6 K. At these temperatures the plasma is very dynamic. Radiative cooling is very probably the dominant energy loss mechanism. At a density of 10^{10} cm^{-3} the radiative cooling time is estimated to be about 30 s. This is fast compared to the lifetime of a blinker event and

implies a continual supply of 10^5 K plasma either through local heating of the transition region or from the corona.

We consider a simple time-dependent model that can represent any plasma in which radiative loss dominates the energy balance. This could represent gas cooling from the corona or plasma cooling after an impulsive heating event, for example shock heating.

The modelling has been done with the ionization and cooling code described by Innes (1985). The evolution of the gas temperature is derived from the energy equation

$$\frac{5p}{2T}\frac{dT}{dt} + \frac{5p}{2(1+y_e)}\frac{dy_e}{dt} = Q_{rad}. \quad (3)$$

The gas pressure, p, is assumed constant and related to temperature, T, number density of atoms, n_a, and electrons, n_e, by $p = n_a(1.0 + y_e)kT$ where $y_e = n_e/n_a$ and k is Boltzman's constant. In Eq. (3) the ratio of specific heats $\gamma = 5/3$ which provides the $\gamma/(\gamma - 1)$, i.e. $5/2$ factor.

The ionization enters through the radiative loss function Q_{rad}. At 10^5 K, the recombination rate is at least an order of magnitude slower than the cooling rate and therefore the ionization evolution is coupled to the plasma evolution.

$$\frac{1}{n_e}\frac{d\mathbf{y}}{dt} = \mathbf{R}\cdot\mathbf{y} \quad (4)$$

where $\mathbf{y}$ are the ion densities relative to n_a and $\mathbf{R}$ is the temperature dependent ionization rates matrix.

Given the ionization, the line emissivity η_l is computed from

$$\eta_l = n_a y_i Y_u A_{ul} \quad (5)$$

where y_i is the ion fraction of the emitting ion, Y_u is the fraction of these ions in the upper level of the line and A_{ul} is the line transition probability. Finally the emissivity over time, t_{cool}, is integrated to give an expected intensity from the cooling plasma:

$$I_l = \int_0^{t_{cool}} \eta_l dt. \quad (6)$$

The ionization and cooling code was developed for studying postshock emission in low density plasma. In order to apply the results to high density transition region plasma, the computed line intensities have been scaled to transition region densities by multiplying by the ratio of the upper level population density at 10^{11} cm^{-3} and 1 cm^{-3}. This ratio was obtained by calculating level populations at 10^5 K with the CHIANTI library of routines.

Two sets of models, listed in Table 4, were considered. The first are cooling coronal models, the CxEx models. In these the gas is initially assumed to be in ionization equilibrium at the model temperature (e.g. 2×10^6 K) and allowed to cool and recombine to a lower temperature of 10^4 K. The second set are the sudden heated models, the HxEx models. In these the ionization is taken to be in equilibrium at 5×10^4 K. Then the plasma is suddenly heated, maintaining ionization to the model temperature. Subsequently the ionization and radiative losses are tracked as the plasma first ionizes and cools then recombines and cools. In all cases, the initial density starts at 5×10^9 cm^{-3} and the plasma cools under constant pressure so the density increases as it cools.

Table 4. Model results, showing intensities normalised to O III

Model	Mg IX	O V	O IV	O III
C2E6	3.0	15	8.1	1.0
C5E5	5.5(-5)	14	8.2	1.0
C1E5		1.7(-3)	0.4	1.0
H2E6	3.0	16	8.2	1.0
H5E5		19	9.0	1.0
H1E5		1.4(-4)	0.16	1.0

Such a simple model is clearly not able to exactly reproduce the observed line ratios. The O V/O IV ratio is almost a factor 2 too large and the O V/O III ratio about a factor 3–4 too large. The strength in this approach is that it illustrates how insensitive such a cooling model is to initial conditions. As long as the plasma is cooling from a temperature above 5×10^5 K, the oxygen line ratios are the same. They are independent of density, initial gas state or exact heat input mechanism. The Mg IX to O line ratios remain unchanged if the gas is heated above 2×10^6 K.

We conclude that the brightening is caused by an increase in density or an increase in the filling factor of cooling plasma.

6. Summary

Before making comparisons to other forms of quiet Sun transient activity, we produce here a summary of the findings of the above investigation:

1. We confirm the existence of extreme ultraviolet blinkers which are particularly clear in the transition region temperature lines from O V, O IV and O III. The intensity enhancements are commonly of order 10–40% for the O V measurements, 10–60% for O IV and 10–40% for O III, with average intensity enhancements of 48%, 43% and 28%, respectively. The most extreme case recorded for the O V data registered an enhancement of over 500%.
2. The blinker events are less clear in the lines from the hotter Mg IX and Mg X ions, which show little, if any, increase. The average enhancements are 4% and 7%, respectively, and the maximum enhancements in these lines was 27% and 44%.
3. The blinker events are also less clear in the cooler line from He I, which again shows almost no increase with an average enhancement of 8% and a maximum enhancement of 56%.
4. The duration of an O V blinker varies significantly, with most events lying in the 400–1600 second range. However, a long tail of longer-duration events gives an average blinker duration of almost 2400 s (40 min). Comparisons to anticipated plasma cooling times firmly establish that there is a continuous energy input throughout the blinker event.
5. The analysis method does not allow a consideration of blinker events of duration less than 300–400 s and of brightenings showing an increase in intensity of under a factor of

1.1. Thus, large numbers of weaker intensity and/or short-lived blinkers may exist.
6. The analysis suggests a blinker onset rate of $1.24\,s^{-1}$ for the entire solar surface, giving 3,000 blinker events in progress on the Sun at any point in time.
7. We do not find any evidence of sympathetic blinker activity, i.e. events triggered by previous events.
8. Although we do show one case suggestive of periodic blinker activity, an analysis of delays between blinker events does not suggest that this is common.
9. An examination of the spectral line ratios suggests that the blinker intensity enhancements are predominantly due to increased density or filling factor rather than temperature.
10. Modelling the signatures using a time dependent code has demonstrated that the line ratios are consistent with an increase in density or filling factor in a plasma cooling from a temperature above 5×10^5 K.
11. An estimate of the average thermal energy of a blinker has been made (2.1×10^{25} erg) but when considered with the blinker frequency and distribution, this energy is not sufficient to heat the corona. It is noted that this is only a measure of the thermal energy and that it does not cater for kinetic energy in accelerated particles, wave energy, energy at temperatures (wavelengths) not detected by the emission lines under examination etc....
12. From the example of the 4 December 1997 data of Sect. 3, we find evidence that the blinker sites are found in the extreme ultraviolet network, and are believed to be at the junction of more than two network cells.

This study has been predominantly concerned with basic time-intensity and spectral behaviour, with a view to establishing some plasma characteristics for the blinker events. Several areas have not been investigated here, or have not been considered fully. These include the analysis of velocity information through the detection of Doppler shifts which will be the subject of a further report. The spatial characteristics, such as a thorough analysis of the locations of blinkers with respect to the network and the size and spatial structure of blinkers in the EUV are, again, the subject of further study.

7. A comparison to other quiet sun phenomena

The current work is an extension of that by Harrison (1997a). It confirms his findings with a much more extensive observation sequence and analysis. Since the earlier report was based on the analysis of only a handful of events, it is not surprising that some features of the observed blinker activity are different. For example, we now have a much clearer picture of the distributions of event durations, enhancement factors etc... The average duration is found to be longer than suspected previously, with many more events identified, and the systematic analysis of the O V time-intensity curves has revealed many more weaker intensity events. The basic finding of both this and the earlier report is that we have a class of extreme ultraviolet brightening in the quiet Sun network which is extremely common, of subflare intensities, and does not result directly in million degree temperatures.

There have been other reports of quiet Sun transient activity and it is important to consider whether the activity reported is related to the blinker events discussed here.

Perhaps the first report of blinker activity was made by Vernazza et al. (1975) using the Harvard College spectrometer on Skylab. They examined a time series of EUV quiet Sun data and reported variations in intensity of up to 50% in times as short as 1 minute, but stressed that they were not periodic. They used a 'stop' mode where a 5x5 arcsecond area was monitored with no raster, sampling every 40 ms over 7 wavelengths. This early report is entirely consistent with the current data. They reported that the maximum effect was in the transition region lines and that very few brightenings were seen in the Mg X 625 Å data. They report typical durations of only 70 s, which is short compared to the events discussed in the current work. However, the CDS observations were made using a rastered image approach, not a single point 'stare' sequence. Although both approaches are valid, the raster ensures that spatial properties are considered, i.e. apparent increases in intensity are not driven by bright regions rotating into the fixed location. On the other hand, the Vernazza et al. approach allows the detection of shorter-lived events.

Porter et al. (1987) examined quiet Sun transient activity using the C IV 1548 Å line observations from the UVSP experiment on the Solar Maximum Mission. They detected both long-duration and short-duration brightenings, the former being associated with X-ray bright points. They noted that the short-duration events were detected throughout the network and even in the cell interiors, and stressed that many of the events had durations shorter than the 2 minute cadence time of their rasters. They suggested that the brightenings were associated with the velocity events detected by Brueckner and Bartoe (1983) (see below), though it is clear that many of the velocity events do not in fact display intensity increases. Whether these UV observations are related to the blinkers discussed above, or are a UV signature of the Brueckner and Bartoe velocity events is not clear. A discussion of the blinker relationship to these velocity events, now detected by the SUMER experiment on SOHO, is given below.

Recently, Berghmans et al. (1998) produced a study of extreme ultraviolet quiet Sun intensity events using the SOHO Extreme Ultraviolet Imaging Telescope (EIT). With this instrument they were able to view a large area of the quiet solar disc with a cadence of about a minute. An analysis of several hours data from the He II line at 304 Å and the Fe XII line at 195 Å formed at 80,000 K and 1,600,000 K, respectively, revealed many sporadic subflare brightenings. The EIT instrument is not a spectrometer but filters out narrow bands around the emission lines in question. Thus, there is no spectral resolution and there may be contributions from adjacent emission lines. In addition, data are only available from the two temperatures, and these observations were not simultaneous.

Berghmans et al. suggest that the He II band brightenings are equivalent to the blinker events reported by Harrison (1997a)

and in this paper. The He II line dominates the emission in that band so the blinker events reported by Berghmans et al. are at a lower temperature than those seen in the oxygen lines in this report. However, there is little doubt that they are witnessing the same events. They report a global blinker birth rate, from the He II data at 20–40 s^{-1} whereas the current paper suggests 1.24 s^{-1}. These are rather different. However, given the errors in projecting from the small CDS fields of view to a full Sun, the different sensitivities of the two instruments, the different wavelengths and the different observation methods, one might not expect to find an identical birth rate.

The Berghmans et al. report also contains an analysis of the Fe XII data, the brightenings of which they refer to as coronal events and liken to the network flares reported by Krucker and co-workers (see below). They report a global birth rate at these temperatures of 1.2 s^{-1}, over a factor of ten less than for the He II events. From the observations used in this report, these events ought to be seen in the Mg IX and Mg X data, at about 1 and 1.2 million K, respectively. However, for the blinker events, which were defined using the O V data, we only found increases on average of 1.04 and 1.07 for these ions with many events being invisible. Even the brightest show increases of only 1.27 and 1.44. Thus, the current analysis of the quiet Sun data does not identify these events. A separate analysis of the Mg data, i.e. not geared to the detection of O V brightenings, is required to identify and analyse any high temperature events of this kind which may be found in the CDS data used in this study. However, the Berghmans et al. study suggests that we might only find less than 10 such events in the CDS data-set. This will be the subject of a further study; we must determine the relationship or 'non-relationship' between the blinkers and the higher-temperature network flare events.

Krucker et al. (1997) and Benz and Krucker (1998) reported on the recent observations of network flares using Yohkoh X-ray, SOHO extreme ultraviolet and VLA radio observations. Their work is concerned with higher temperature variations than those reported in the blinker work; the Benz and Krucker analysis used the Fe IX/X million K line at 171 Å and the Fe XII 1.2 million K line at 195 Å; Krucker et al. used X-ray emission characteristic of 1.8 million K plasma. Again, if these events had occurred as part of the blinker events studied in this paper, signatures in the Mg IX and Mg X lines would have been detected.

It is extremely important to realise that the analysis of the blinker events in the current paper is driven by the O V analysis, i.e. enhancements in the few hundred thousand K region. Events were identified using the O V line and we have analysed the subsequent event data-set. The million degree transient activity associated with these events is almost non-existent and ought to have been readily identifiable using the Mg IX and Mg X data. As noted above, the Berghmans et al. work identified significant differences between the coronal and transition region events suggesting that only less than 10 of the former would be seen in the data-set examined here. It is clear that Krucker and co-workers, and Berghmans and co-workers have identified a form of high temperature activity and, at least for the present, the results suggest that we must talk of two different classes of event, the blinker (which is an enhancement dominated by transition region lines) and the less-frequent network flare (which is dominated by high temperature lines). The current work suggests that the two are not related in general but much more observation and analysis is required to confirm or reject this.

In another quiet Sun study, Gallagher et al. (1999) also used the CDS instrument to look for intensity variations. Unlike the current study, they did not raster; they used a single slit and stared at a set location for 90 minutes. They found numerous transient brightenings in the He I 584 Å (20,000 K) and O V 629 Å (250,000 K) lines with common durations between 80 and 200 s and dimensions of 6,000–10,000 km. They noted that the variations are most evident in the network, but are detected to a lesser extent in the internetwork. They did not take any higher temperature data. In a sense, this recent report is complementary to the current study. The rasters used in the present work mean that we are not able to look for intensity variations in the EUV using the CDS observations at less than about 150 s. This single-slit location method allows the examination of shorter duration events. One does have to remember that a single-slit observation of this kind does suffer from apparent intensity variations as solar features rotate into the field of view, but it is clear that the more rapid variations in particular are real. One must conclude that the events detected by Gallagher et al. are, in particular, the short-duration tail of the blinker distribution reported in the current paper.

Perhaps of most importance here is to establish the relationship between the blinker events and the so-called explosive events reported by Innes et al. (1997a,b). Both event types have been reported as being common features of the network in the ultraviolet. The explosive events have been detected using SOHO (Innes et al.) as well as with the HRTS instrument (e.g. Brueckner and Bartoe, 1983). They are predominantly from transition region lines and, rather than being brightenings, they are characterised by significant velocity shifts. Typically such events are short lived (60 s), small scale (about 2 arcseconds) and occur at a rate of about 600 s^{-1} over the Sun's surface. Typical line of sight velocities during the events are 150 km s^{-1}, often bidirectional.

The fact that the explosive events and the blinkers are both so common and that they occur in similar network locations would suggest that there is an intimate link. The explosive events appear to be much smaller and shorter-lived. However, initial inspections of the emission line profiles of the CDS data used for this study do not reveal flows up to 150 km s^{-1} within the blinker data. Analysis of velocity data continues in an effort to pursue this matter and a full report will be given later. However, typical spectral line fits in the blinker events using the CDS data have so far revealed either no clear velocity shifts or modest velocities of up to a maximum of 20 km s^{-1}. This is confirmed by Gallagher et al. (1999). It should be pointed out that the CDS observations have an spatial element of order 2 arcseconds at best and that the use of the 4 arcsecond wide slit for the blinker observations might mean that the small-scale explosive events are simply washed out due to the intensity from areas

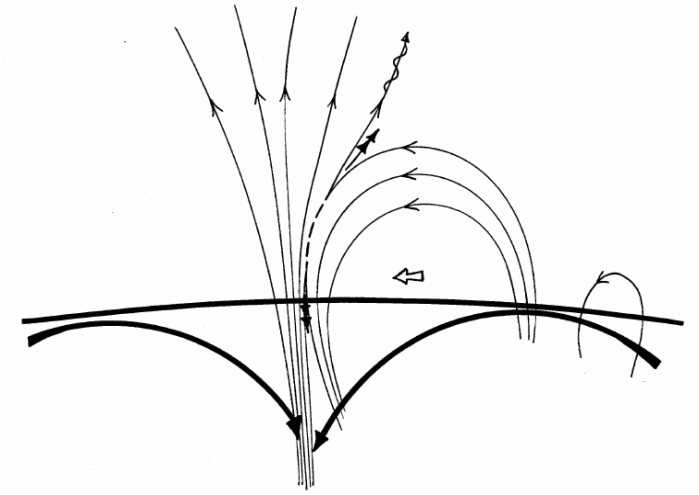

Fig. 13. A blinker model showing the interaction of a closed magnetic feature migrating across a convection cell and interacting with the concentrated magnetic flux in the network (see text).

surrounding the explosive event. The explosive event may well be part of the process which we have called the blinker in EUV.

It is clear that the blinkers, the network flares and the explosive events are all features of quiet Sun activity and it is imperative that we identify each class and the relationships between them. For two of the blinker observation sequences listed above we have coincident observations from the SUMER ultraviolet spectrometer on SOHO and from a close analysis of the CDS and SUMER data we hope to perform a thorough investigation of the blinker, explosive event relationship. For the present, we simply identify the blinker, explosive event relationship as one outstanding problem.

8. A blinker model

A cartoon model which caters for many features of blinker activity is given in Fig. 13. The photosphere runs through the middle of the figure and the thick arrows below the photosphere indicate the convective plasma flow at the supergranular level. In the upflow region one might expect to see magnetic flux emergence, with loops extending into the corona due to buoyancy or overshoot. This is indicated by the existence of a closed loop in the right hand side of the figure. Since the plasma and field are frozen into one another in normal solar conditions, the emerged flux will travel with the convective flow, to the left in this case. This will result in magnetic merging at the network where we know the magnetic flux is concentrated. One could imagine a variety of magnetic configurations which might arise. In the case shown in Fig. 13, the opposing fields of the loop and the network field lead to the creation of a neutral line and formation of a current sheet at the location shown dashed in the figure. Some energisation of the local plasma could be identified as a result of the dissipation of the current sheet. Below the photosphere we have a high beta plasma so it is easy to envisage the merging fields being driven to a situation where magnetic reconnection may occur, as suggested by the figure. This could result in particle acceleration and heating, flows and the generation of waves as indicated on the right-most open field line in the figure.

There are many observables in such a picture. Initially one might expect to see the migration of magnetic fragments towards the region which will be the site of the blinker. The blinker itself will occur predominantly over the downflow region, or in the network; this is the case. One can imagine line of sight effects leading to blinker activity apparently within the cells, and it is perfectly possible that in some cases loops could reconnect as they migrate to the network or cell boundary, again giving events within the cells. However, the dominant location would be the network.

The energetics of such a system must be considered in the light of the blinker characteristics given above. We do not normally see high temperatures, so the current sheet dissipation and any thermalisation of the particle acceleration must not cause significant rises in temperature. The increase in density seen by CDS could be an apparent increase in density due to the merging of the magnetic fields, i.e there is an increase in emission measure at transition region temperatures due to the merging of fields carrying plasma at those temperatures in the network.

The duration of the event is probably driven more by the convective flow of the cell than anything else and the durations and the rare periodic blinker events may tell us something about the nature of the cell flow speeds. The twin-headed arrows coming from the reconnection sites are indicating the expulsion of jets which could be the explosive events seen by Innes et al. (1997a,b) and, certainly, the magnetic configuration of that part of our picture matches the model put forward by Innes et al. In addition, if Alfvén waves emanate from the reconnection site, they may travel into the corona along the field lines as indicated. These could be a prime driver of the solar wind. However, we would not detect any Alfvén wave activity in the blinker or explosive event data taken thus far since it has been concentrated on disc target areas. Future observations on the limb may be critical for the identification of such activity. Of course, the open field lines of Fig. 13 may feed into overlying closed loops in which case the ascending wave activity may dump energy into plasma trapped in larger coronal systems. Similarly, the jets may thermalise at a site away from the prime blinker site and this needs to be investigated in some detail.

So, it is important to note that although we see an event which has little immediate impact at typical coronal temperatures, the full impact on the solar atmosphere cannot be assessed from the thermal energy only. We must identify and investigate the nature of associated flows and wave activity.

We are beginning to understand the true nature of a basic, common process in the Sun's low atmosphere which may play a significant role in solar wind acceleration and plasma heating. We note that the scenario suggested has similarities to the model proposed by Axford and McKenzie (1992) which suggested that solar wind acceleration may result from the frequent merging of closed loops with the network fields. For this reason, we have

already embarked on a consideration of that model with the plasma characteristics identified in this work.

9. Concluding remarks

This is the first thorough spectral analysis of blinker activity. It has revealed the basic nature of blinker events and allowed the first steps in producing a blinker model. Although the thermal energy contained in the blinker events is not enough to heat the corona, it is important to develop a full model of blinkers, including all forms of energy and related activity in order to assess the full impact on the corona. Comparisons to other observed transient events in the solar atmosphere point towards some crucial questions which must be addressed by the observers, using multi-instrument analyses. However, we have an ubiquitous transient event type in the low solar atmosphere and, in the light of our goals to understand fully coronal heating and solar wind acceleration, a full understanding of the role of these events must be pursued.

Acknowledgements. CDS was built and is operated by a consortium led by the Rutherford Appleton Laboratory and including the Mullard Space Science Laboratory, the NASA Goddard Space Flight Center, Oslo University and the Max-Planck-Institute for Extraterrestrial Physics, Garching. SOHO is a mission of international cooperation between ESA and NASA. DHB acknowledges partial support from the Portuguese Fundação para a Ciência e Tecnologia through grant PESO/P/PRO/1196/97 and PESO/P/INF/1197/97.

References

Arnaud M., Rothenflug R., 1985, A&AS 60, 425
Athay G., White O.R., 1978, ApJ 226, 1135
Axford W.I., McKenzie J.F., 1992, In: March E., Schwenn R. (eds.) Proc. Solar Wind Seven. Pergamon Press, p. 1
Benz A.O., Krucker S., 1998, Solar Phys. 182, 349
Berghmans D., Clette F., Moses, D. 1998, A&A 336, 1039
Brooks D.H., Fischbacher G.A., Fludra A., et al., 1999, A&A 347, 277
Brueckner G.E., Bartoe J.-D.F., 1983, ApJ 272, 329
Dere K.P., Landi E., Mason H.E., Monsignori-Fossi B.F., Young P.R., 1997, A&AS 125, 149
Feldman U., 1992, Physica Scripta 46, 202
Gallagher P.T., Phillips K.J.H., Harra-Murnion L.K., Baudin F., Keenan F.P., 1999, A&A 348, 251
Harrison R.A., 1997a, Solar Phys. 175, 467
Harrison R.A., 1997b, In: Proc. 5th SOHO Workshop: The Corona and Solar Wind Near Minimum Activity. ESA SP-404, 7
Harrison R.A., Sawyer E.C., Carter M.K., et al., 1995, Solar Phys. 162, 233
Harrison R.A., Fludra A., Pike C.D., et al., 1997, Solar Phys. 170, 123
Innes D.E., 1985, Ph.D. Thesis, University of London
Innes D.E., Inhester B., Axford W.I., Wilhelm, K., 1997a, Nat 386, 811
Innes D.E., Brekke P., Germerott D., Wilhelm K., 1997b, Solar Phys. 175, 341
Krucker S., Benz A., Acton L.W., Bastian T.S., 1997, ApJ 488, 499
Porter J.G., Moore R.L., Reichmann E.J., Engvold O., Harvey K.L., 1987, ApJ 323, 380
Raymond J., Doyle J.G., 1981, ApJ 247, 686
Summers H., 1994, Joint European Torus Report, Atomic Data and Analysis Structure. JET-IR (94)-06
Vernazza J.E., Foukal P.V., Huber M.C.E., et al., 1975, ApJ 199, L123